Papers

Electron Beam Pumped Broad-Band Diatomic and Triatomic Excimer Lasers

FRANK K. TITTEL, SENIOR MEMBER, IEEE, GERD MAROWSKY,
WILLIAM L. WILSON, JR., MEMBER, IEEE, AND MICHAEL C. SMAYLING

(Invited Paper)

***Abstract*—The spontaneous and stimulated emission characteristics of three recently reported broad-band blue-green rare gas-halide excimers, XeF ($C \rightarrow A$) at 486 nm, Xe_2Cl at 518 nm, and Kr_2F centered at 436 nm, are reviewed. The influence of different halogen donors and buffer gases as well as optimization of both the gas mixture and optical resonator configuration for wavelength tuning were studied. The kinetic mechanisms which describe the formation and quenching of Xe_2Cl^* are discussed. Problems with achieving optimum gain as well as understanding both molecular and atomic absorptions in electron beam excited rare gas-halide mixtures are detailed.**

I. INTRODUCTION

SINCE 1975, numerous excimers have been reported that are capable of generating high power laser reduction in the visible and ultraviolet spectrum [1]-[5]. The relatively simple techniques required to pump such lasers, as well as their demonstrated high efficiency, have made them useful lasers in many interesting applications. Recently, there has been interest in exploring the broad bandwidth emission, which is observed from several diatomic and triatomic excimers as wavelength tunable laser sources (see Fig. 1). Alternatively, conversion of narrow-band UV excimer laser emission into longer wavelength tunable dye laser radiation has been demonstrated [4].[1] Wavelength tuning of an excimer was first achieved over a 6 nm tuning range with the Xe_2 laser centered at 172 nm [6]. With either a prism or diffraction grating as the wavelength selecting element, a tuning range of 4 nm for an Ar_2 excimer laser at 127 nm [7] and ~2 nm for ArF, KrF, XeCl, and XeF ($B \rightarrow X$) excimers [8], [9] has been achieved. In this paper, the general characteristics of three new electron beam pumped lasers, XeF ($C \rightarrow A$) [10], Xe_2Cl [11], and Kr_2F [12], capable of broad-band tunability will be discussed. Fig. 2 summarizes the complexes associated with high pressure mixtures of the rare gases argon, krypton, and xenon with the halogens fluorine and chlorine. The pure rare gas excimers, Ar_2^*, Kr_2^*, and Xe_2^* with UV emissions at 126, 146, and 172 nm, respectively, are shown in the first column. The other columns list their respective exciplex transitions: the short wavelength $B \rightarrow X$ transition, the longer wavelength broad-band $C \rightarrow A$ transition, and the emission of the triatomic exciplex. For Ar_2F^* and Xe_2F^*, the wavelengths listed are the center of the fluorescence emission, whereas the data given for Kr_2F^* and Xe_2Cl^* correspond to the center of the laser emission, as obtained in the experiments described below.

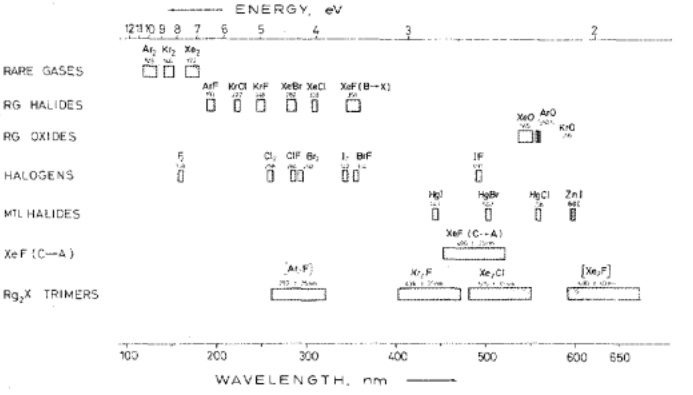

Fig. 1. Wavelengths and tuning ranges of the various rare gas, rare gas-halide, rare gas-oxide, halogen, mercury halide, and broad-band RgX and Rg_2X excimer lasers. For Ar_2F and Xe_2F, the spectral ranges of fluorescence are indicated.

Manuscript received July 20, 1981. This work was supported by the Office of Naval Research, the National Science Foundation, and the Robert A. Welch Foundation.

F. K. Tittel and W. L. Wilson, Jr. are with the Department of Electrical Engineering and Rice Quantum Institute, Rice University, Houston, TX.

G. Marowsky is with the Max-Planck Institute, Gottingen, Germany.

M. C. Smayling was with the Department of Electrical Engineering and Rice Quantum Institute, Rice University, Houston, TX. He is now with Texas Instruments, Houston, TX.

[1] Commercial excimer laser pumped dye laser systems are offered by several manufacturers.

0018-9197/81/1200-2268$00.75

RARE GAS	EXCIMER	EXCIPLEX (B→X)	EXCIPLEX (C→A)	TRIMER
Ar	Ar_2 126nm	ArF 193nm	ArF	Ar_2F 290nm
Kr	Kr_2 146nm	KrF 248nm	KrF 285nm	Kr_2F 430nm
Xe	Xe_2 172nm	XeCl 308nm	XeCl 345nm	Xe_2Cl 520nm
		XeF 351nm	XeF 485nm	Xe_2F 630nm

Fig. 2. Rare-gas halide complexes and their associated emission wavelengths. The $C \rightarrow A$ transition of ArF has not yet been identified.

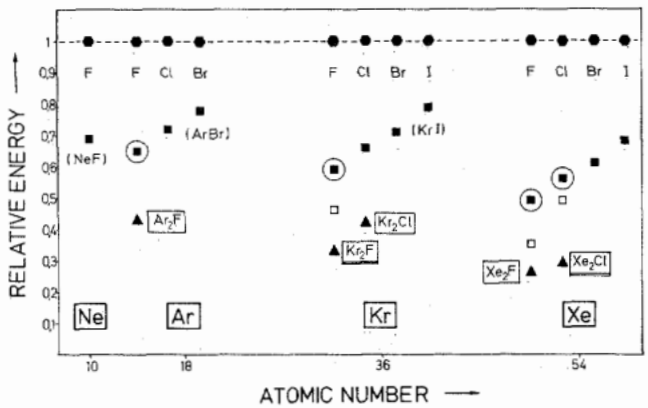

Fig. 3. Relative dissociation energy of rare gas-halide excimers versus the atomic number of the rare gas; ● represents the pure rare gas excimers such as Ne_2^*, Ar_2^*, Kr_2^*, and Xe_2^*; ● represents a $B \rightarrow X$ exciplex; □ represents a $C \rightarrow A$ exciplex; ▲ stands for triatomic exciplexes. The double lines indicate those trimers which have shown laser action.

II. Chemical Physics

Homogeneously broadened excimer emission bands have been observed on the long wavelength side of most $B \rightarrow X$ electronic laser transitions as incidental companion fluorescence [1], [13]. These emission spectra are attributed to diatomic $C \rightarrow A$ transitions and triatomic homonuclear and heteronuclear rare gas-halide excimers.

In Fig. 3, the dissociation energies of the rare gas-halide excimers listed in Fig. 2 are plotted versus atomic number of the rare gas. Each energy is normalized to the dissociation energy of its respective rare gas excimer Ar_2^*, Kr_2^*, and Xe_2^*. The unstable Ne_2^* and NeF^* exciplexes have been added for completeness. From this figure it is apparent that: 1) the dissociation energy of the RgX exciplex decreases with increasing atomic number, and 2) the dissociation energy increases regularly for a particular rare gas with F, Cl, Br, and I. This diagram is useful in the search for wavelength positions of new unknown candidates for broad-band $C \rightarrow A$ transitions (marked by the rectangular symbols) or new trimers (marked by the triangular symbols) such as Ar_2Cl^* or the bromides of Kr and Xe.

Schematic potential energy curves for the various RgX^* and Rg_2X^* excimer lasers under consideration are shown in Fig. 4.

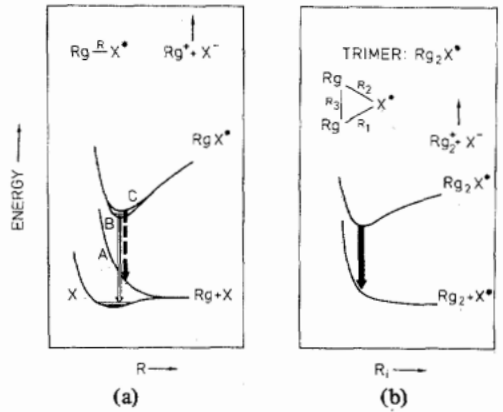

Fig. 4. Chemical structure and potential energy diagrams for a typical (a) diatomic RgX* and (b) Rg_2X^* triatomic molecule.

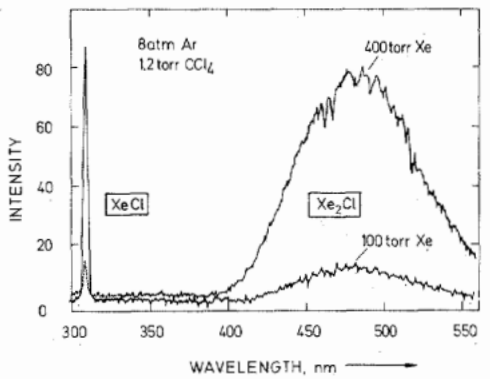

Fig. 5. Xenon pressure dependence of XeCl ($B \rightarrow X$) and Xe_2Cl fluorescence spectra.

Excimer lasers operate on electronic transitions involving a bound ionic excited state and a repulsive, or at most weakly bound, lower state that rapidly dissociates. The lowest electronic level is designated the X state, with higher levels labeled A, B, C, etc. [Fig. 4(a)]. Due to the weakly bound nature of the X state, the allowed $B \rightarrow X$ transition is inherently narrow banded. The $C \rightarrow A$ transition, however, terminates on the highly repulsive A state, which gives rise to the broad bandwidth of this transition. For the triatomic exciplex [Fig. 4(b)] Rg_2X^*, the ground state is repulsive, similar to the A state of the dimer, and thus, the emission is characteristically broad banded.

The formation of the trimer depends on several factors. It is strongly enhanced by increasing both the buffer gas pressure and the concentration of the rare gas. High pressure favors excimer formation by increasing the recombination rate of atomic excited states into the molecular upper level. Fig. 5 depicts the effect of xenon pressure by showing the relative Xe_2Cl^* fluorescence emission for two different Xe pressures in electron beam excited $Ar/Xe/CCl_4$ mixtures. The $XeCl^*$ fluorescence intensity is not only reduced by opening the formation channel towards Xe_2Cl^*, but also by increased nonradiative quenching of $XeCl^*$ due to the higher Xe partial pressure, as discussed in Section VI.

Because of the broad bandwidth characteristics of these excimers, the stimulated emission cross section of the bound-free transitions is small. Therefore, pumping rates larger than those

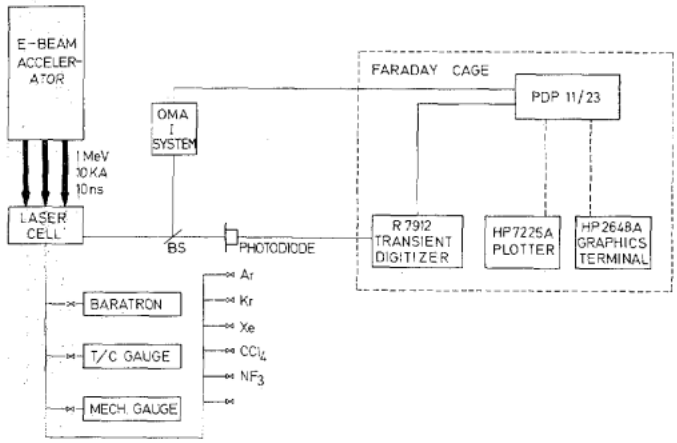

Fig. 6. Block diagram of the experimental arrangement and the data acquisition system.

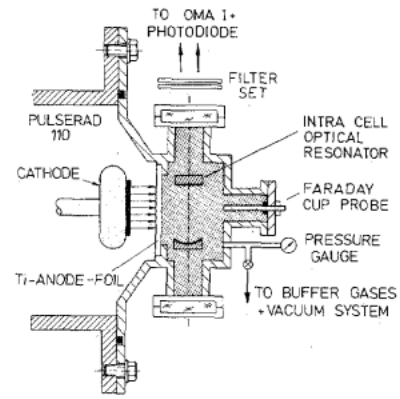

Fig. 7. Schematic diagram of the transverse electron beam pumped laser cell.

of atomic level lasers are necessary for reasonable gain. This requires intense electron beam or other powerful pumping excitation (fast discharge or optical) of the excimer species in order to achieve large excited state populations. The formation of the excimer relies primarily on ion recombination and chemical reactive collisional processes involving excited rare gas species and an appropriate halogen donor.

III. Experimental Details

The basic experimental arrangement, illustrated in Fig. 6, consists of an electron beam excitation source, a high pressure laser cell, and various electrical and optical instrumentation. Direct electron beam excitation is one of the most general techniques for pumping excimer lasers [1]-[3] on account of the high peak powers available (in excess of 10^3 MW/cm^3), broad spectral applicability, and scalable and proven technology. Efficiencies for conversion of electrical energy into excited states of the main buffers is close to 50 percent. Furthermore, electron beam excited reactions can be conveniently transferred to discharge laser systems. Different techniques are available for coupling the electron beam into the laser medium. These include transverse, radial, or longitudinal pumping of the laser cell. In this paper, we employ transverse excitation of the active media by means of an electron beam produced by the field emission diode of a Physics International Pulserad 110 electron beam generator. This machine is capable of producing 15 kA pulses of 1 MeV electrons with an 8 ns pulse duration. A device such as the Pulserad 110 is especially useful as a pump source for excimer lasers, since the short output pulse may not only be used to pump potentially low-gain laser media, but the short excitation pulse permits detailed studies of pertinent reaction kinetics. The electron beam is transversly injected into the laser cell through a 50 μm thick titanium foil which serves as the anode of the field emission diode, as well as a pressure barrier to separate the laser media from the high vacuum diode region. The laser cell and field emission diode are shown in Fig. 7, and are described in detail in [14]. Several electrical monitors are useful in determining how well the *e*-beam generator is performing. A Marx bank voltage probe and a Rogowski coil (for measuring diode current) monitor the basic machine performance. A calorimeter and Faraday probe, which can both be mounted inside the laser cell, monitor energy deposition and current density along the optical axis. With an 8 cm X 1 cm cathode and 6 atm of argon, the current density is ~100 A/cm^2 and the energy density is ~2 J/cm^2 at a distance of 2.5 cm from the anode foil.

The laser cell is connected to an all stainless steel gas-vacuum manifold. The quality of the gases used in the experiments and the filling techniques employed are important factors in obtaining consistent experimental results, since quenching by even small amounts of impurities can be severe. The rare gases used—neon, argon, krypton, and xenon—were of research grade, 99.995 percent pure. Halogen donors such as CCl_4 and NF_3 were of spectrophotometric grade, with a purity of 99+ percent. The halogen donors were allowed to flow into the reaction cell slowly to permit precise pressure measurement of less than 0.1 torr. The pressure was monitored with a capacitive MKS baritron gauge. The gas manifold was evacuated to less than 10 mtorr between fillings of the gas constituents. Buffer gases were introduced into the cell through high-flow regulators to allow turbulent mixing of the halogen donor and the rare gas. Because of deterioration of the halogen donor molecules, refilling of the laser cell was necessary after a few shots.

The cell arrangement shown in Fig. 7 has several features which are important for achieving laser output from low-gain media. The intracell resonator, comprised of two high-reflectivity mirrors separated by 10 cm, eliminates reflection losses which would occur at window surfaces in the case of external optics. Internal optics also allow the use of a short cavity length to decrease the roundtrip transit time. The resonator may be conveniently aligned from outside the cell, since the mirrors are held by flexible bellows mounts. Alignment is necessary after every laser shot to insure consistent performance. The bellows mounts are made versatile so that they can be adapted to hold a variety of cavity optics, including mirrors, prisms, and gratings. The optimum cavity configuration consisted of a high reflectivity (>99 percent) curved mirror (r = 2 m) and a flat output coupler (2-5 percent) with its optical axis 2.5 cm from the anode. Wide-band (±15 nm) dielectric coatings were used with a protective SiO_2 outer layer to prevent attack by fluorine and chlorine on the sensitive optical coating. For such a resonator, the volume of the active region was only about 0.04 cm^3, but this geometry insured alignment stability against the *e*-beam induced shock wave.

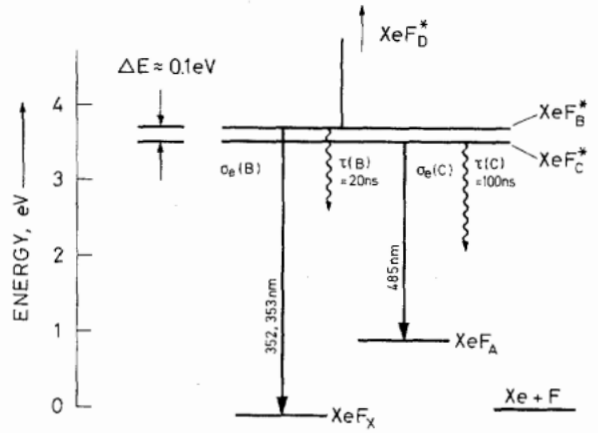

Fig. 8. Energy level scheme of the diatomic excimer XeF ($B \rightarrow X$) and XeF ($C \rightarrow A$) transitions.

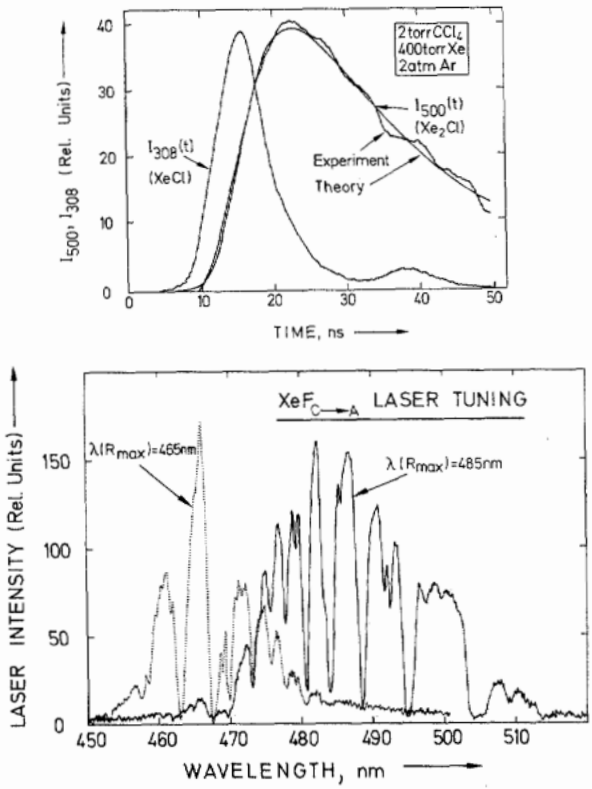

Fig. 9. Spectra of XeF ($C \rightarrow A$) laser showing tuning effects using reflectors with maximum reflectivity centered at 465 nm and 485 nm, respectively.

Unstable resonators would yield a much larger interaction volume, but laser threshold conditions would be difficult to obtain with the low-gain excimers.

The optical emission of the electron beam excited rare gas-halide mixture in the laser cell could be monitored in several ways. Time integrated spectral data were recorded with a Princeton Applied Research optical multichannel analyzer (OMA 1) using a model 1254D intensified vidicon detector. Temporal data were obtained simultaneously with a fast vacuum photodiode (ITT F4000 S5) or a photomultiplier (RCA C31000B). Narrow-band interference filters were used to obtain temporal characteristics in a limited spectral range. The signal from the photodiode was recorded with a Tektronix R7912 transient digitizer. Careful electrical and X-ray shielding of the detection apparatus minimized noise that resulted from firing the *e*-beam machine. Both the transient digitizer and the OMA 1 were interfaced to a DEC PDP 11/23 minicomputer system, controlled by means of an HP 2648A graphics terminal, as shown in Fig. 6. Temporal and spectral data reduction and feature extraction were accomplished with software routines developed for this purpose.

IV. The XeF ($C \rightarrow A$) Laser

As a first example of a broad-band tunable excimer laser, the XeF ($C \rightarrow A$) laser centered in the blue-green at 486 ± 20 nm is briefly discussed. This laser has been pumped photolytically [15], [16] and by both electron beam [10], [17] and discharge [18], [19] excitation. Continuous broad-band tunability and an output energy in excess of 6 J have been reported in [20]. Amplification by injecting tuned dye laser pulses is described in [21]. The relatively high gain of XeF ($C \rightarrow A$) [22]-[24] accounts for its successful operation under such diverse conditions. The relevant energy levels of the $C \rightarrow A$ and $B \rightarrow X$ transitions of XeF are given in Fig. 8. Contrary to the usual case, the C state lies about 0.1 eV (700 cm^{-1}) below the B state in this system [25]-[27]. The ratio of C and B state quantum yield is about 0.1 [28]. The small energy difference between the B and C states may be used to enhance the population density of the C state by cooling the gas mixture to below room temperature [29]. Heating the mixture increases the B state population, and thus favors the $B \rightarrow X$ transition at 351 and 353 nm. Fig. 9 demonstrates the broad-band tunability of the $C \rightarrow A$ transition using a wide-band 100 percent reflector, and two 2 percent output couplers centered at 465 and 485 nm. The figure shows a potential tuning range of 65 nm, from 450 to 515 nm, for an optimized mixture of 16 torr Xe, 8 torr NF_3, and 6 atm Ar. An intracell Littrow prism or a high efficiency grating could also be used to tune the laser output, but only in a longitudinally pumped cell with increased gain length [30]. The strong modulation of the laser output shown in Fig. 9 is due to transient absorption processes, and will be discussed in Section VIII. The laser pulses occur in the afterglow of the electron beam excitation because of initial molecular absorptions arising from the argon buffer gas and the long ring-up time due to the limited gain [31], which delay the laser action by ~35 ns [10]. An interesting feature of the XeF $C \rightarrow A$ transition occurs when a very high-Q resonator cavity is used. A sudden increase in the output power by as much as two or three orders of magnitude, accompanied by enhanced spectral and temporal narrowing, is observed. This may be due to enormously increased photon flux inside the high-Q cavity. In this case, a few of the absorption features (indicated by 1-3 in Fig. 10) have been bleached out and appear in emission. A possible explanation for this high output could be that the extremely high-Q cavity for the $C \rightarrow A$ transition might lead to the channeling of all of the inversion energy into the $C \rightarrow A$ bound-free emission. Assuming a Boltzmann temperature distribution between the C and B states, and a level spacing of ~0.1 eV, one can only account for a factor of 50 increase, which is about 10 times too small for the observed increase in output intensity. An alternative explanation

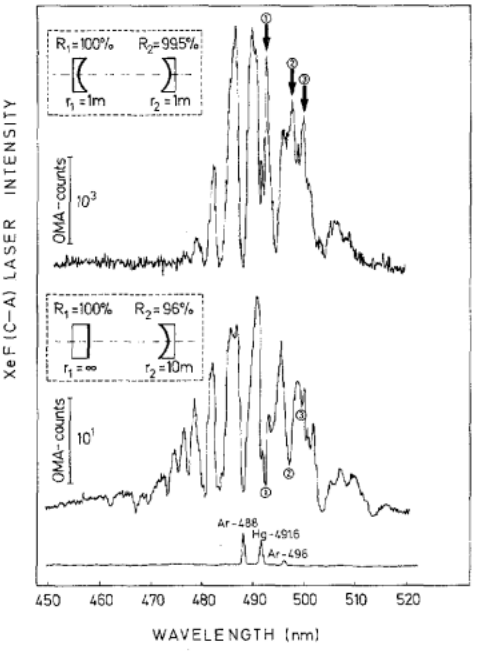

Fig. 10. Influence of cavity-Q on XeF ($C \rightarrow A$) laser intensity. For high-Q cavity (upper spectrum) laser intensity increases by a factor of 10^2. At spectral positions ①, ②, and ③, absorption features of low intensity spectrum are reversed into emission lines. Mercury and Ar^+ laser lines are included for calibration.

would be that the high intercavity photon flux may lead to nonlinear bleaching [32] of an unusually broad-band absorption feature of unknown origin. In any event, the large output powers observed suggest that for efficient utilization of the $C \rightarrow A$ transition, either a cavity dumping technique or a fast injection procedure might prove very useful.

V. The Triatomic Rare Gas-Halide Excimers: Xe_2Cl and Kr_2F

In addition to emission from the rare gas-halide excimer RgX^*, broad-band emission is observed at longer wavelengths from triatomic exciplexes Rg_2X^* [1], [14], [33]-[36], as described in Section II. Such trimers are primarily formed by three-body collisions between the excimer RgX^* and a rare gas. The ionic potentials of the excited states of these trimers have been calculated using *ab initio* computations [36]-[39] and a "diatomics in molecules" (DIM) approach [40]. Table I lists the homonuclear rare gas-halide triatomic molecules, as well as such important parameters as the emission wavelengths for transitions to the repulsive ground state [Fig. 4(b)], the bandwidth $\Delta\lambda$, and the radiative lifetime (reciprocal Einstein A coefficient) τ_{rad}. It is immediately obvious from Table I that the bandwidths for these bound-free transitions, typically 50–80 nm, are much larger than the 1–2 nm for the mainline $B \rightarrow X$ transition. The radiative lifetimes are also much longer, typically 100–200 ns for the trimers, as compared to 4–40 ns for the diatomic excimers. Of the 10 trimers listed in Table I, only Xe_2Cl [11] and Kr_2F [12], [41] have been observed to lase so far. The spectral and temporal fluorescence characteristics of high pressure $Ar/Xe/NF_3$, Ar/NF_3, and $Ar/Xe/CCl_4$ mixtures were evaluated. These mixtures were typically composed of a few torr of a halogen donor, several hundred torr of

TABLE I
Spectroscopic Properties of the Triatomic Rare Gas Halides

Rg_2X	λ (nm)	$\Delta\lambda$ (nm)	τ_{rad} (ns)	References
Ne_2F	145[a]	–	–	[37]
Ar_2F	290	45	220	[b], [49], [c]
Ar_2Cl	246	30	–	
Kr_2F	420	70	>130	[b], [11], [33], [48], [55]
Kr_2Cl	325	30	>500	[13]
Kr_2Br	318	–	–	[20]
Xe_2F	630	100	~200	[b]
Xe_2Cl	490	80	>135	[b], [13], [43], [45], [70]
Xe_2Br	430	80	250	[13], [20]
Xe_2I	375	–	–	[13]

[a] Calculated, possible spectrum in [37].
[b] This work.
[c] R. Sauerbrey and H. Langhoff, private communication, $\tau_{rad}[Ar_2F] = 230 \pm 100$ ns.

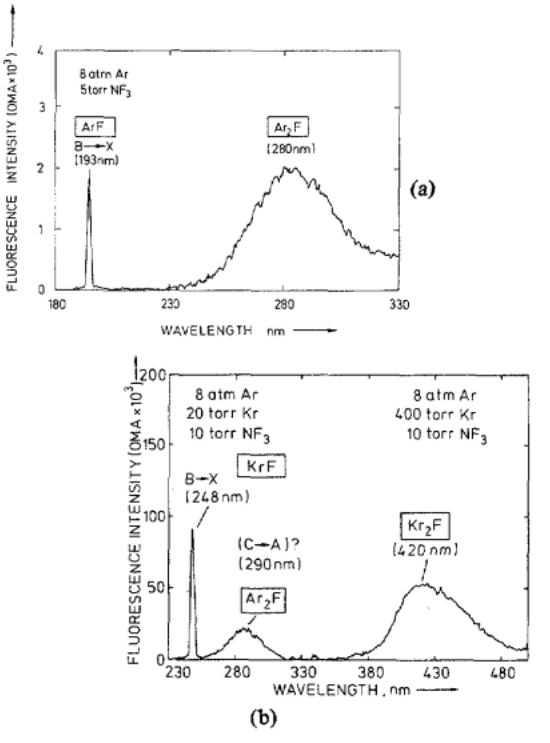

Fig. 11. Fluorescence spectra of (a) Ar_2F and ArF ($B \rightarrow X$) and (b) of Kr_2F and KrF ($B \rightarrow X$). In the case of (b), the fluorescence peaks of Ar_2F and KrF ($C \rightarrow A$) are superimposed at 290 nm.

a rare gas, and several atmospheres of a buffer gas. Composite fluorescence spectra of the excimers studied in this work are shown in Figs. 11 and 12. Such fluorescence measurements served to determine various spectroscopic and laser parameters. In addition, kinetics and optimum gas composition of the broad-band exciplex media were studied under fluorescence conditions.

A laser spectrum for Xe_2Cl is shown in Fig. 13. The laser spectrum is characterized by spectral narrowing with the FWHM decreasing from 80 to 13 nm. Furthermore, the intensity of the stimulated emission increases compared to fluorescence intensity. In addition, the peak laser intensity is red shifted by 30 nm from the fluorescence peak. This is partly caused by the λ^4 gain dependence [1] and partly by the cavity reflectors centered at 520 nm. Cavity enhanced atomic ab-

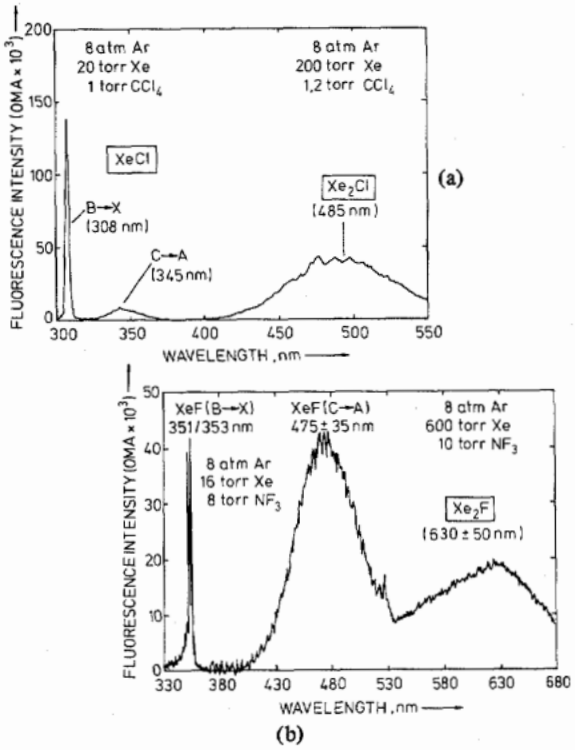

Fig. 12. Fluorescence spectra of (a) Xe_2Cl, XeCl ($B \rightarrow X$), and XeCl ($C \rightarrow A$) and (b) Xe_2F, XeF ($B \rightarrow X$), and XeF ($C \rightarrow A$).

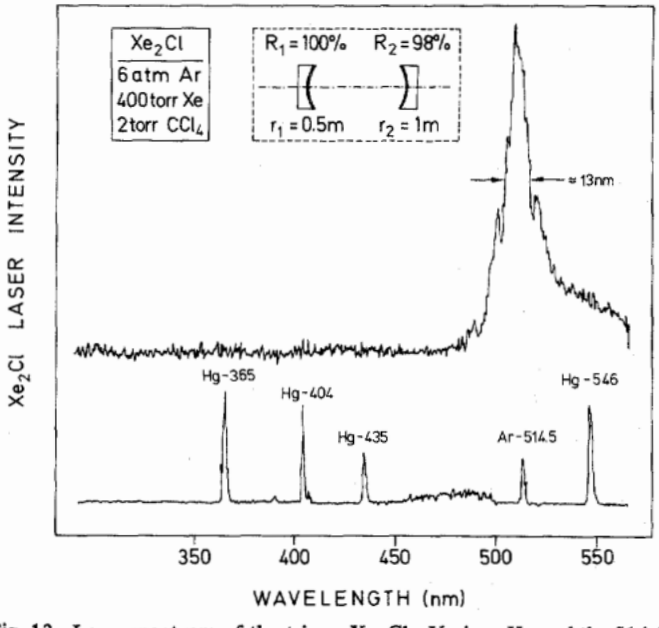

Fig. 13. Laser spectrum of the trimer Xe_2Cl. Various Hg and the 514.5 nm argon ion laser line are indicated for calibration of the OMA I spectrum.

sorption lines are apparent as in the case of the XeF ($C \rightarrow A$) laser. Fig. 14 shows typical normalized temporal characteristics of the UV and visible fluorescence and laser output from a high pressure Ar/Xe/CCl_4 mixture. The laser pulse exhibits temporal narrowing compared to the fluorescence pulse, and is considerably delayed (by ~35 ns) from the *e*-beam pulse due to buffer gas transient absorptions. Furthermore, the Xe_2Cl^* emission occurs delayed with respect to the UV fluorescence

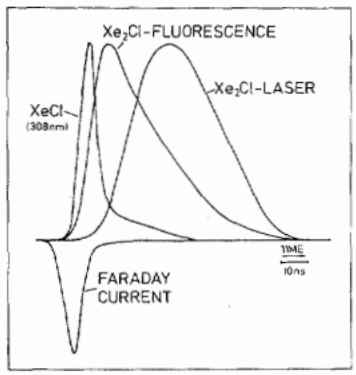

Fig. 14. Temporal composite of Xe_2Cl laser and fluorescence, XeCl ($B \rightarrow X$) fluorescence, and the *e*-beam pump pulse.

pulse and the laser output reaches its maximum peak intensity later than the Xe_2Cl fluorescence peak. As discussed previously, the delay of the laser pulse is a consequence of the long ring-up time of the cavity oscillation as discussed in [31]. A series of experiments was conducted to find optimal conditions for maximum laser output. The gas mixture was studied in detail over the following ranges: CCl_4, 0.4-3 torr; Xe, 100-800 torr; Ar, 2-10 atm. The strong influence of CCl_4 and Xe partial pressure on the laser output is evident in Fig. 15(a) and (b). At 200 torr of Xe, the laser intensity had a sharp peak at 1.2 torr CCl_4 with the peak shifting for higher Xe pressures. As can be seen, the effective pressure range for CCl_4 and Xe is quite limited. The argon buffer gas had a surprising effect on the intensity, as Fig. 15(c) shows. The saturation at high Ar pressures reflects both a limitation in the formation of Xe_2Cl^* and absorptions by excited molecular argon [42]. Neon and nitrogen were also used as buffer gases to isolate some of the effects of argon absorption. However, the trimer did not achieve threshold laser conditions for up to 10 atm of N_2, and showed only weak laser action with up to 12 atm of neon. Other chlorine donors species such as Cl_2, HCl, $CHCl_3$, CH_2Cl_2, and CH_3Cl were also tried, but CCl_4 proved to be better in terms of optimizing laser performance.

Besides spectral and temporal narrowing, the trimer output showed spatial narrowing as well. The laser beam divergence was measured to be about 8 mrad. As in the case of XeF ($C \rightarrow A$), tuning was accomplished with cavity reflectors of different center wavelengths.

The other triatomic laser Kr_2F [12], although somewhat weaker than the Xe_2Cl laser, showed all the characteristics expected for stimulated emission behavior, which were discussed in detail for the Xe_2Cl laser. The peak laser output occurred with 10 torr NF_3 as the halogen donor, while the output showed no real maximum for both Kr and Ar but, rather, increased with pressure. Atomic absorptions by krypton metastables were identified in the laser spectrum.

VI. Kinetics of Triatomic Excimers

The energy transfer and excited state kinetics for trimers is complex, especially for electron beam pumping [1]-[4]. The detailed kinetic route by which the excimer is formed depends upon the excimer, the halogen donor molecule, the excitation conditions, and the partial pressures of the constituent gases.

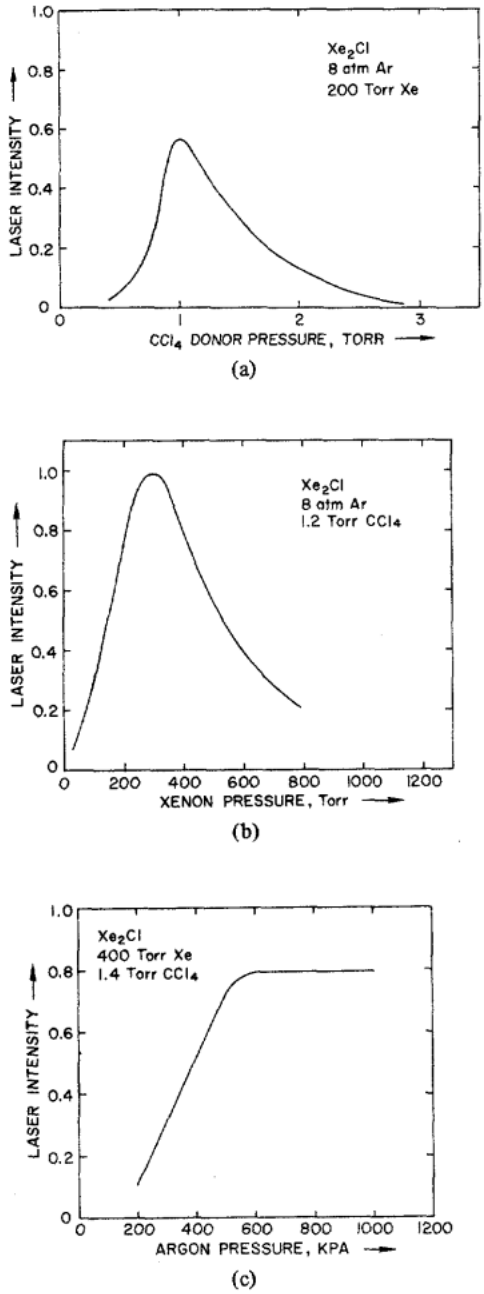

Fig. 15. Dependence of Xe_2Cl laser intensity upon (a) CCl_4 concentration, (b) xenon concentration, and (c) argon concentration.

The main excitation mechanism takes place via three-body reactions of excited and ionized excimers. In this paper, we limit the discussion to Xe_2Cl^* kinetics based on temporal fluorescence measurements of electron beam excited $Ar/Xe/CCl_4$ mixtures [43]. It is apparent from Fig. 14 that the Xe_2Cl^* fluorescence peak occurs after the UV fluorescence had effectively decayed to zero. From this observation and previous work [44], [45] it may be concluded that the diatomic excimer $XeCl^*$ is a precursor in the reaction chain leading to the formation of Xe_2Cl^*, subsequent to channeling of initial electron energy into the excited dimer state. Such a conversion of RgX^* into Rg_2X^* has been considered as the predominant formation mechanism for other ionic and substitutive reactions involving two or three bodies for Ar_2F, Kr_2F, and Kr_2Cl [13], [46]-[50].

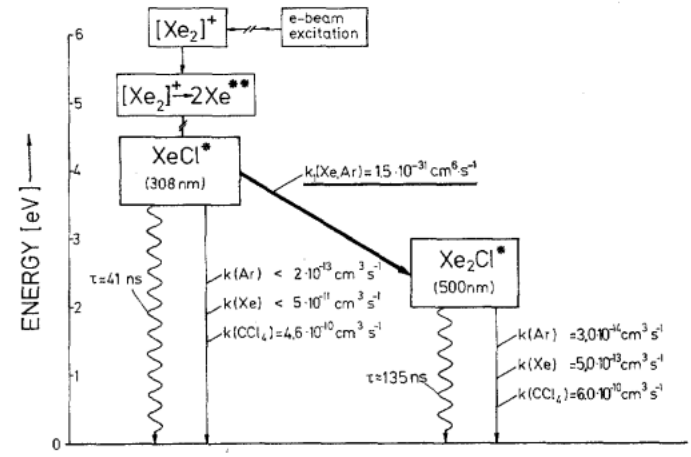

Fig. 16. Schematic diagram of the Xe_2Cl kinetic process. Radiative lifetimes and quenching rate constants are also depicted.

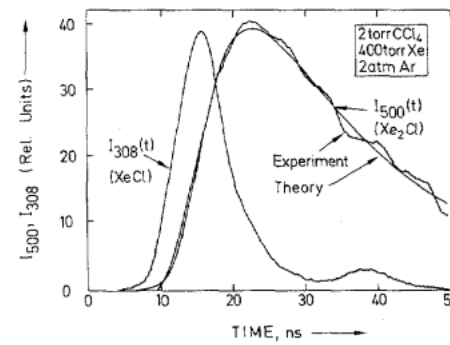

Fig. 17. Comparison of experimentally observed Xe_2Cl fluorescence pulses and calculated pulses based on the kinetics model of Fig. 16 [36].

A reaction scheme for the formation of Xe_2Cl^* from $XeCl^*$ via a termolecular reaction is illustrated in Fig. 16. For XeCl the production of Xe_2Cl corresponds to an alternative decay channel, together with radiative decay and collisional quenching due to Ar, Xe, and CCl_4, with quenching rate coefficients as indicated in Fig. 16. The $XeCl^*$ emission data appear to indicate a further possible quenching mechanism, with $k_{XeCl}(Ar, Xe) \approx 4 \times 10^{-30}$ cm$^6 \cdot$ s^{-1} by another three-body collisional process that involves a highly unstable intermediate species such as $ArXeCl^*$ [51], [52]. For the pressure range required for optimum trimer fluorescence, $XeCl^*$ suffers severe quenching by the high xenon pressures. The termolecular formation mechanism may be tested in several ways, as discussed in [44]. For example, Fig. 17 shows the good agreement between the experimentally measured and calculated Xe_2Cl pulses for a mixture of 2 atm Ar, 400 torr Xe, and 2 torr CCl_4.

Rate constants for the formation reaction and for several termolecular quenching reactions of Xe_2Cl^* have been measured [43] and are given in Fig. 16. The value of the formation constant $k_1(Ar, Xe)$ was found to be $1.5 \pm 0.5 \times 10^{-31}$ cm$^6 \cdot$ s^{-1}. The dominant loss process for both $XeCl^*$ and Xe_2Cl is quenching by the halogen donor CCl_4. Quenching by argon and by xenon is less severe. The quenching conditions play an important role in determining the laser operating conditions, as was shown in Fig. 15. The rate of collisional quenching of the

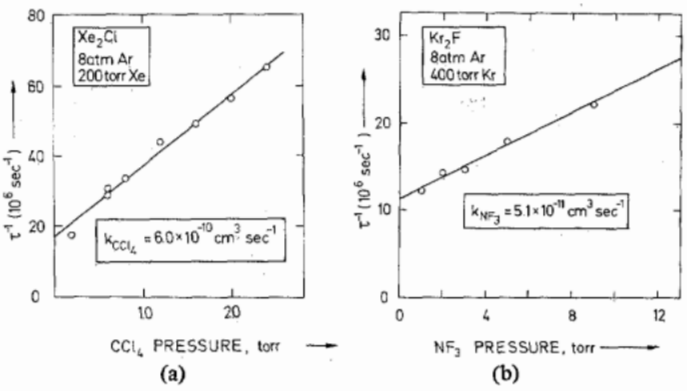

Fig. 18. Stern-Volmer plots of (a) Xe_2Cl^* against CCl_4 pressure, and (b) Kr_2F against NF_3 pressure.

trimers was established by measuring the decay constant τ for a number of mixtures containing constant amounts of two of the gases but different amounts of the third component. Some of the experimental data are shown in Figs. 18 and 19. In Fig. 18, the Xe_2Cl and Kr_2F decay frequency τ^{-1} is plotted as a function of the CCl_4 and NF_3 pressures, respectively. From the slopes, $k^q_{CCl_4}$ and $k^q_{NF_3}$ were calculated as $(6 \pm 1) \times 10^{-10}$ cm$^3 \cdot$ s^{-1} and 5×10^{-11} cm$^3 \cdot$ s^{-1}, respectively. Thus, NF_3 is a much less severe quencher than CCl_4. This observation is substantiated by the halogen donor pressure dependence of the fluorescence of Xe_2Cl and Kr_2F as shown in Fig. 19. Hence, it is possible to employ much higher NF_3 pressures than CCl_4 to optimize fluorescence intensity. However, as discussed in the previous section, a search for another chlorine donor has not been successful thus far. The radiative lifetime of the donors can be estimated from the zero intercept in Figs. 18 and 19. This intercept contains contributions due to collisional quenching of Xe_2Cl^* by Xe and Ar, and of Kr_2F^* by Kr and Ar. However, when these were subtracted, the respective radiative lifetimes were computed as 135 and 130 ns. The postulated trimer formation mechanism predicts only a limited efficiency for the production of Xe_2Cl from XeCl in the absence of an intermediate heteronuclear excimer species. The laser output powers for electron beam pumped triatomic excimers so far are limited by the relatively small formation rate, and by the presence of transient molecular and atomic absorptions.

VII. Optical Gain Considerations

A critical issue of the performance of low-gain lasers such as Xe_2Cl, Kr_2F, and XeF $(C \rightarrow A)$ is the relationship between the gain of the excimer transition and absorptions from other molecular or atomic species. The gain may be measured experimentally by a variety of methods. A comparison of three of these methods is presented in [22]. This reference describes gain measurements made on XeF by a shutter technique, in which different volumes of the gas are excited by the *e*-beam, by a mirror method, in which amplified spontaneous emission is used, and a direct measurement using a CW laser probe beam. Gain may also be determined by measuring the ring-up time of the laser pulse [28], [31]. Table II provides a comparison between the calculated and measured gains for each of the laser mixtures studied. The data for the $B \rightarrow X$ transitions of XeF

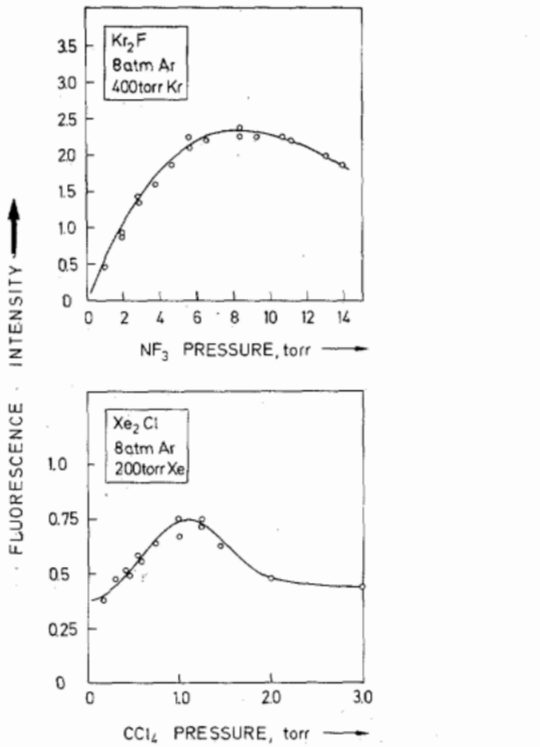

Fig. 19. Pressure dependence of Xe_2Cl^* and Kr_2F^* fluorescence on the halogen donor partial pressure.

are included for comparison. It is immediately evident from this table that the broad-band excimer lasers possess far less gain than their narrow-band rare gas-halide counterparts. This is due to the smaller stimulated emission cross section, and the fact that the trimers and the $C \rightarrow A$ dimers represent decay channels for the primary diatomic exciplexes. Except for Kr_2F, the general agreement is good. In the case of Kr_2F, the gain measurement was made at a wavelength corresponding to a strong absorption in the laser spectrum. Hence, little or no gain would be expected, and in fact, only absorption was observed [53], [54]. The optical gains reported for XeF $(C \rightarrow A)$ [22], [23] and Xe_2Cl [55] are in agreement with those measured in this work even though the experimental conditions were quite different. The lower gain for discharge pumped XeF $(C \rightarrow A)$ [17] is a result of the lower pumping power used.

In the absence of absorbers, the unsaturated gain coefficient g of an excimer system may be calculated using fluorescence data in the expression [1], [2]

$$g = \sigma N^* = \frac{1}{8\pi c \tau} \frac{\lambda^4}{\Delta\lambda} N^*$$

where σ is the stimulated emission cross section, λ is the central wavelength of the transition, $\Delta\lambda$ is the bandwidth (FWHM) of the fluorescence spectrum, N^* is the excited state population density in the upper laser level, and c is the velocity of light. The gain data of the broad-band transition lasers in Table II are based on the probe-beam measurement of g_o for XeF $(C \rightarrow A)$ [23]. For this excimer, $N^* = 7 \times 10^{15}$ cm^{-3} has been calculated, and this figure has then been used to compute the other excited state densities based on comparable OMA and diode measurements, taking into account the spectral response of the detectors.

TABLE II
COMPARISON OF CALCULATED AND EXPERIMENTAL GAIN DATA

Excimer	σ, cm^2 × 10^{-17}	g_{calc}, cm^{-1}	g_{exp}, cm^{-1}
Kr_2F	0.7	0.013[a]	–
Xe_2Cl	0.8	0.024	0.027[b], 0.025 [55]
Ar_2F	0.2	0.002	–
XeF ($C \rightarrow A$)	1.1	0.07	0.05 [22], [23], 0.01 [17], 0.3 [22]
XeF ($B \rightarrow X$)	50	–	

[a] Only absorption was observed in [53] and [54].
[b] This work.

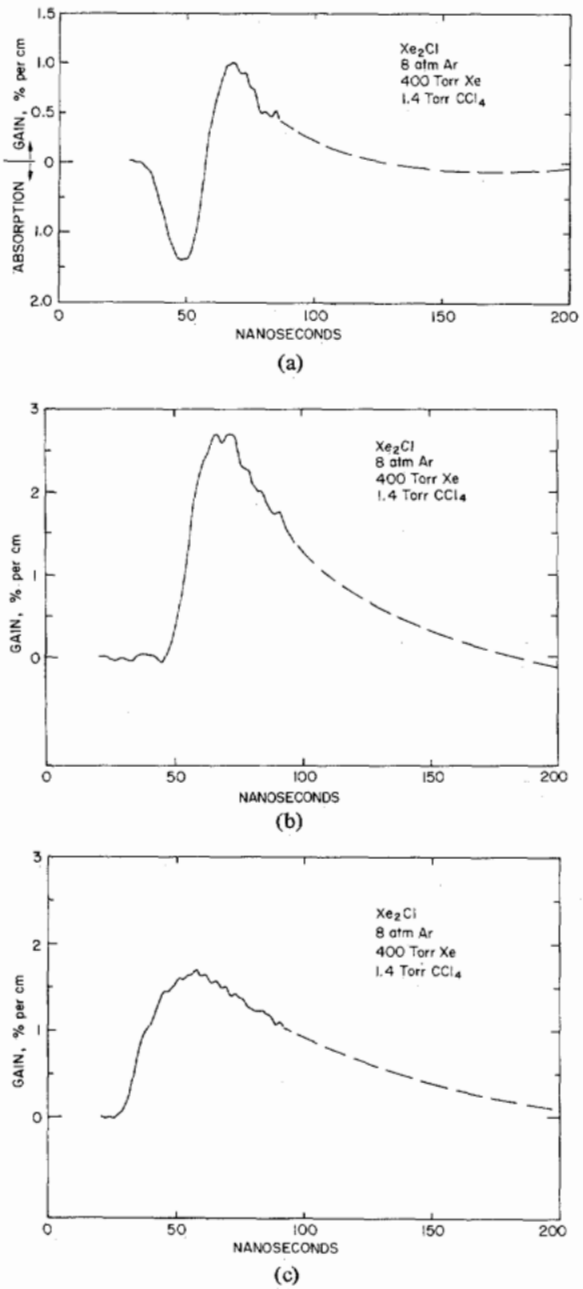

Fig. 20. Temporal behavior of Xe_2Cl gain with optical axis (a) 1.5 cm from foil, (b) 2.5 cm from foil, and (c) 3.5 cm from foil (vertical pass).

Because of the availability of several Ar^+ laser lines in the Xe_2Cl excimer band, and the possibility of increasing the sensitivity of the gain measurement by many horizontal or vertical

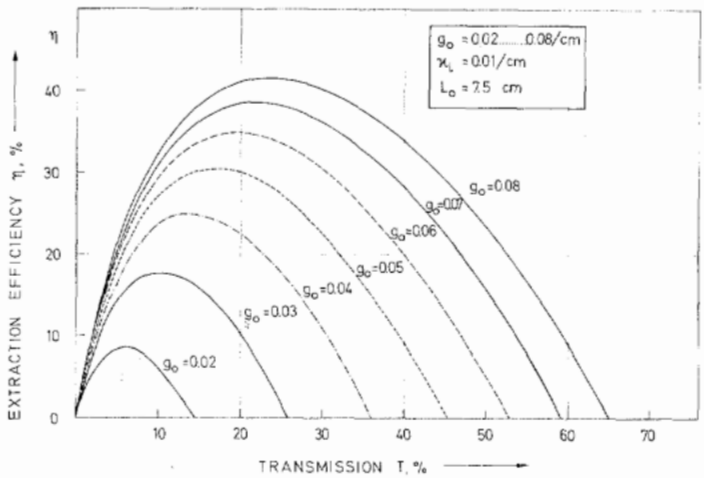

Fig. 21. Calculated extraction efficiency of e-beam pumped low-gain excimers as a function of output coupling for the indicated value of g_0. Internal losses are characterized by $\kappa_i = 0.01$/cm (details in [47]).

multiple transits (3–5 passes) through the excimer medium, the direct probe method is particularly useful. This method makes it possible to measure conveniently both the magnitude and temporal behavior of the effective optical gain. Fig. 20 shows that the net gain varies strongly as a function of distance from the anode foil. Near the anode foil, a strong initial molecular absorption in the immediate afterglow of the pump pulse is seen, followed by a weak gain of ~ 1 percent/cm. The intermediate case, at the optic axis, shows gain and absorption canceling initially, followed by a strong gain of 2.7 percent/cm. The lack of initial absorption was unexpected, although the delay in the gain peak corresponds well to the delay in the laser output. At the furthest distance from the anode [Fig. 20(c)] no initial absorption was present, and a gain of 1.7 percent/cm occurred soon after the e-beam pump pulse. The gain measurements on Xe_2Cl at 514.5 nm are useful, since they confirm the gain calculations as well as provide insight into the competition between e-beam induced molecular absorption and population inversion.

So far all the output power from the broad-band excimer lasers is in the kilowatt range, primarily due to the small active mode volume available from the stable resonator. However, it should be pointed out that even in low-gain systems, the extraction efficiency in terms of photons coupled out divided by the number of excited states produced by the particular transition could be as high as 50 percent with an appropriate choice of output couplers. Fig. 21 depicts the dependence of extraction efficiency ξ versus transmission of the output coupler,

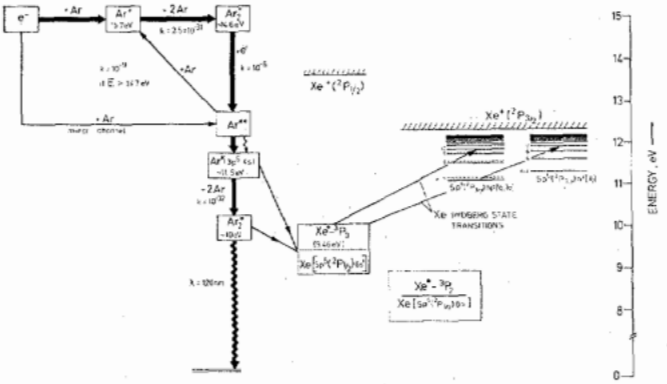

Fig. 22. Kinetic scheme leading to atomic absorption from $^3P_0$ xenon metastables to high-lying Rydberg levels.

under the assumption of steady-state conditions for various gain figures ranging from $g_o = 0.02\ \text{cm}^{-1}$ to $g_o = 0.08\ \text{cm}^{-1}$ and $L = 7.5$ cm, as discussed in detail in [56]. Fig. 21 shows that the output powers of the broad-band lasers could be enhanced by nearly one order of magnitude by selection of an optimum output coupler.

VIII. Molecular and Atomic Absorption by Electron Beam Pumped Broad-Band Rare Gas Halides

The existence of transient absorption in electron beam pumped rare gas halides limits the performance of excimer lasers by lowering extraction efficiency and limiting scalability. Two of the most prominent characteristics of low-gain XeF ($C \rightarrow A$), Xe_2Cl, and Kr_2F electron beam excited lasers is that stimulated emission is delayed by broad-band ionic absorbing species and the presence of a large number of intense absorption lines present in the emission spectrum [2], [10]-[12], [28], [57]. The broad-band absorbers have been identified as molecular in origin [42], and come from the argon buffer gas in the form of dimers such as Ar_2^+. The absorbing excited molecules are created at the onset of electron beam excitation, and have a lifetime of 10-20 ns. This absorption seriously limits the laser efficiency even though the excited state production efficiency is very high. Thus, laser action occurs in the afterglow regime of the electron beam pulse. The transient nature of the molecular absorption is clearly shown in Fig. 20. The absorption at 515 nm is on the order of 30 percent/cm at 8 atm of Ar [42]. The other absorption has been identified as involving longer living excited atomic species, notably the rare gas metastables, which survive for hundreds of nanoseconds. These atomic metastables can give rise to discrete absorption involving transitions to excited Rydberg states [58]-[60].

Metastable states are most likely created by excitation from excited argon species, following the kinetic chain listed below (also shown in Fig. 22):

$$e^- + \text{Ar} \rightarrow \text{Ar}^+ + 2e^-$$

$$\text{Ar}^+ + 2\text{Ar} \rightarrow \text{Ar}_2^+ + \text{Ar}$$

$$\text{Ar}_2^+ + e^- \rightarrow \text{Ar}_2 \rightarrow \text{Ar}^{**} + \text{Ar}$$

$$\text{Ar}^{**} + 2\text{Ar} \rightarrow \text{Ar}_2^* + \text{Ar}.$$

Both Ar_2^* and Ar^{**} are capable of interacting with Xe to form Xe^* [61], [62] by the following reactions:

$$\text{Ar}^{**} + \text{Xe} \rightarrow \text{Xe}^* + \text{Ar}$$

$$\text{Ar}_2^* + \text{Xe} \rightarrow \text{Xe}^* + 2\text{Ar}.$$

Xenon has two excited metastable states, $^3P_2$, $\{5p^5(^2P_{3/2})6s[3/2]_2\}$, and $^3P_0$, $\{5p^5(^2P_{1/2})6s'[1/2]_0\}$. In addition, there are two other excited states with $5p^56s$ configuration, $6s[3/2]_1$ ($^3P_1$) and $6s'[1/2]_1$ ($^1P_1$), but they have allowed dipole transitions to the ground state, and are thus short-lived in situations where the xenon concentration is low. The $^3P_2$ metastable is located at 8.3 eV, whereas the $^3P_0$ metastable state is at 9.5 eV. These states may absorb radiation and undergo resonant transitions to higher excited Rydberg levels near the ionization limit, as depicted in Fig. 22. For large principal quantum numbers n, the Rydberg atom is hydrogenic in the sense that it consists of a single electron moving in an orbit around a unit charge. Some possible transitions from xenon metastables are to the $nf(3/2)_1$, $nf(5/2)_1$, $np(1/2)_1$, and $np(3/2)_1$ excited states. The selection rule is that the parity must change during the transition, and that $\Delta J = \pm 1, 0$ [55]. For principal quantum number n up to about 12, the location of the observed excited states has been tabulated [63]. The energy levels of Rydberg states with higher principle quantum numbers can be calculated using a quantum defect model. For such a model, one calculates the ionization energy of the higher states using the expression

$$E_{\text{ionization}}(\text{eV}) = \frac{\text{Ry}}{(n-\delta)^2}$$

where Ry is the Rydberg constant (13.6 eV) and δ is the quantum defect, which is calculated from known lines with the expression

$$\delta = n - \sqrt{\frac{13.6}{\text{IP} - E_n(\text{eV})}}.$$

IP is the ionization potential of the metastable (12.1 eV for Xe) and E_n is the energy of a known level with principle quantum number n.

In order to identify the absorption lines in the laser spectrum of XeCl ($C \rightarrow A$) Xe_2Cl and Kr_2F, carefully calibrated time-integrated spectra were recorded with the optical multichannel analyzer. Calibration spectra were taken before and after each shot, using mercury emission or argon ion laser lines as reference. A computer program was used to plot the spectra with a calibrated wavelength scale.

Fig. 23 shows typical high-resolution laser spectra for both XeF ($C \rightarrow A$) and Xe_2Cl. Absorptions by Xe metastables have been identified at many wavelengths throughout the excimer laser band. Assignments of the transitions indicated in Fig. 23 were based on data from [57], [58], [63]. Absorption lines identified in Xe_2Cl and XeF ($C \rightarrow A$) laser spectra arising from the $^3P_0$ metastable state are listed in Table III. There was one transition from the $^3P_2$ metastable state to the $7p(3/2)_1$ Rydberg state at 461.3 nm. However, no absorptions originating from the Xe $^3P_1$ level were observed as in [28]. It should be noted that there are other absorption lines visible on the spectra which have not yet been identified.

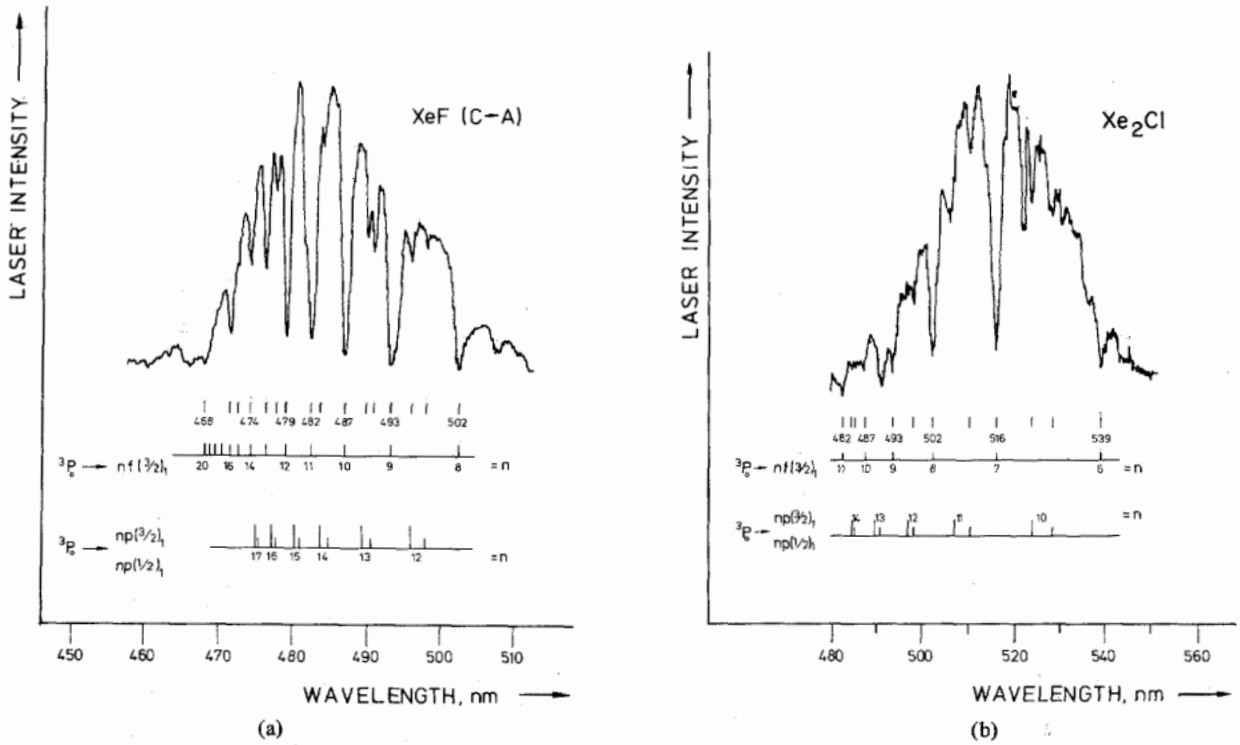

Fig. 23. Laser spectra of (a) Xe_2Cl and (b) XeF ($C \rightarrow A$) showing absorption lines which have been identified as due to transitions between the $^3P_0$ Xe* metastable and high-lying Rydberg states. Both spectra were obtained with optimized rare gas-halide mixtures.

TABLE III
IDENTIFIED TRANSACTIONS BETWEEN XENON $6s'^3P_0$ METASTABLES AND HIGH-LYING RYDBERG STATES

	n	eV	Transition in nm
$nf(3/2)_1$			
	7	11.84	516.4
	8	11.91	502.5
	9	11.96	493.4
	10[a]	11.99	487.1
	11	12.01	482.5
	12	12.03	479.1
	13	12.05	476.5
	14	12.06	474.5
	15	12.07	472.8
	16	12.07	471.5
$np(1/2)_1$			
	11	11.88	509.3
	12	11.94	497.5
	13	11.98	491.1[b]
	14[c]	12.00	484.2
	16	12.04	477.5
	18	12.06	473.4
$np(3/2)_1$			
	10	11.80	619.7
	11	11.88	508.3
	12	11.94	497.3

[a] Values for n = 10–16 calculated using $\delta = 0.043$.
[b] This value differs from a transition of 489.3 which is calculated from the data in [63].
[c] Values for n = 14–18 calculated using $\delta = 3.45$.

The laser spectra of Kr_2F also shows a number of characteristic absorption lines. Some of these can be identified with transitions from krypton metastables to low-level Rydberg states. The emission spectrum of Kr_2F is centered at around 435 nm, whereas the high-lying Rydberg levels have transitions corresponding to around 350 nm. Thus, the overlap of the emission spectrum and the rich region of the absorption spectrum is not as great as in the case of XeF ($C \rightarrow A$) or Xe_2Cl. Transitions from $^3P_2$ to $6p(3/2)_1$ and $6p(1/2)_1$ can be identified, as well as a transition from the $^3P_0$ metastable to the $5f(3/2)_1$ Rydberg level. The unidentified lines may be due to absorption by NF_3 or reaction byproducts.

Additional confirmation of the metastable nature of the absorbing species was obtained by comparing the temporal behavior of the XeF ($C \rightarrow A$) laser at 486 nm, where the OMA spectrum indicates a maximum in output intensity with a corresponding minimum in the spectrum at 487 nm. In both cases, the laser output had the same temporal characteristics. Since the XeF ($C \rightarrow A$) pulse length was greater than 60 ns, the absorption must have remained relatively constant throughout the duration of the pulse. Hence, the initial level of the absorbing species must be metastable on this time scale.

Several attempts were made to reduce the effects of the absorptions. For example, the Kr_2F laser was operated at $-55°C$ to shift the absorption to lower wavelengths [53], [64]. No major change was observed. The XeF ($C \rightarrow A$) and Xe_2Cl lasers were also operated at lower temperatures with different buffer gases such as Ne, Xe, and N_2, but most of the absorption features remained unaffected.

Absorption features are a significant characteristic of *e*-beam excited broad-band excimer lasers. Not only do these absorption lines reduce the total output power from the laser, but they play a significant role in limiting the tunability of the laser. In principle, it should be possible to eliminate a large number of these lines by introducing a quencher for the xenon

metastable ground state. Efforts in that direction have had limited success thus far, although recent work reported in [28] suggests that the atomic metastable absorptions may be quenched by rapid transfer to N_2 when using photolytic excitation at 172 nm with an Xe_2^* radiation source.

IX. Summary

Laser characteristics were studied extensively for the broad-band rare gas-halide excimers Xe_2Cl, Kr_2F, and XeF ($C \rightarrow A$). Since all three excimers have unbound ground states, a spectrally wide emission bandwidth is available for wavelength tuning. Other excimers with wide fluorescence bandwidths—Ar_2F and KrF ($C \rightarrow A$) at 290 nm, XeCl ($C \rightarrow A$) at 345 nm, and Xe_2F at 630 nm—were studied but exhibited gains which were too small to achieve laser threshold in the 10 cm transversely pumped laser cavity used in these experiments. Spectral and temporal fluorescence studies were conducted as an intermediate step in establishing optimum conditions for obtaining laser action, and to derive kinetic constants. A detailed spectroscopic study was performed for Xe_2Cl^*, which yielded formation and quenching rate constants as indicated in Fig. 16. Tuning was achieved for all three excimers by using optics centered at different wavelengths. Efficiencies for these lasers were small because of the small active volume defined by the stable optical resonator geometry. The optical gain for the trimer Xe_2Cl was measured up to 2.7 percent/cm. The gain was delayed by transient absorptions involving the argon buffer gas. In addition, atomic absorptions from metastable lower states to Rydberg upper states were also identified in all the laser spectra. Gain data are listed in Table II, and the xenon $^3P_0$ metastable absorption lines observed in the XeF ($C \rightarrow A$) and Xe_2Cl laser spectra are compiled in Table III.

Several future approaches to the development of tunable broad-band excimer lasers appear to be feasible. For example, other Rg_2X molecules as indicated in Table I, such as Xe_2Br, Kr_2Cl, or Ar_2F, may be studied as potential new laser media. Second, new methods of coupling the *e*-beam energy into the buffer gas should be tried to increase the laser output power. For example, the approach of using optical pumping may be evaluated since it avoids the problem of *e*-beam induced transient absorption effects, as reported in [15], [55]. Eventually, discharge excitation of these laser media may be possible by using optical or X-ray preionization [65] of high pressure rare gas-halide mixtures in view of the difficulty of operating stable discharges in high pressure gases. Recently, supersonic flow-electron beam stabilized discharge excitation of diatomic and triatomic excimers has been proposed [66] to lower the excited species quenching and absorption losses.

Improved energy coupling can be accomplished by longitudinal pumping of the laser cell. In the "λ" arrangement, illustrated in Fig. 24(a), the *e*-beam is coaxial with the laser axis instead of being perpendicular to it. This method of *e*-beam pumping was developed by a group at Sandia Laboratories [67]. A "head-on" version of this design, shown in Fig. 24(b), has been described in [68] and [69]. Although this second configuration is simpler than the "λ" geometry, since no turning coil is needed, it does not allow the use of high quality cavity optics, since the *e*-beam must pass through one of the

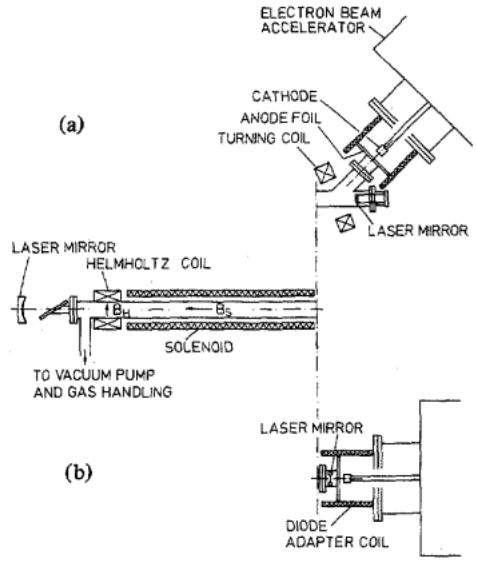

Fig. 24. Longitudinally electron beam pumped laser cell in (a) the λ geometry and (b) the head-on configuration.

cavity reflectors. Preliminary experiments using the λ configuration have yielded three orders of magnitude increase in power for an Ar-N_2 laser mixture as compared to the output when using the transverse cell shown in Fig. 7.

The longer available gain length of the longitudinal arrangement will allow a variety of tuning experiments. Insertion losses encountered by using prisms, gratings, or etalons should not exceed the per pass gain of the medium. This condition is not satisfied for low-gain broad-band excimers pumped transversly. Besides more efficient *e*-beam energy deposition, the longer cell will also permit using reflectors which will greatly increase the active volume, and hence yield much greater laser output power. Such improvements will make broad-band excimer lasers more useful for potential applications on account of their wide wavelength tunability.

Acknowledgment

The authors would like to acknowledge the experimental assistance of G. Zhenhua, and helpful discussions with Dr. G. Glass and Dr. F. B. Dunning. Much of the early work reported here was performed with the assistance of Dr. W. E. Ernst and Dr. R. E. Stickel, Jr.

References

[1] C. K. Rhodes, Ed., *Excimer Lasers.* Berlin: Springer, 1979.
[2] J. J. Ewing, "Excimer lasers," in *Lasers Handbook*, vol. 3. Amsterdam, The Netherlands: North-Holland, 1979.
[3] M. J. Shaw, "Excimer lasers," *Progr. Quantum. Electron.*, vol. 6, pp. 3–54, 1979.
[4] M.H.R. Hutchinson, "Excimers and excimer lasers," *Appl. Phys.*, vol. 21, pp. 95–114, 1980.
[5] I. S. Lakoba and I. S. Yakovlenko, "Active media of exciplex lasers," *Sov. J. Quantum Electron.*, vol. 10, pp. 389–410, 1980.
[6] D. J. Bradley, M.H.R. Hutchinson, and C. C. Ling, "Tunable VUV excimer laser systems," in *Tunable Lasers and Applications*, A. Mooradian, T. Jaeger, and P. Stockseth, Eds. Berlin: Springer, 1976, pp. 40–48.
[7] W. G. Wrobel, H. Rohr, and K. H. Steuer, "Tunable vacuum UV laser action by argon excimers," *Appl. Phys. Lett.*, vol. 36, pp. 113–115, 1980.
[8] T. R. Loree, K. B. Butterfield, and D. L. Baker, "Spectral tuning

of ArF and KrF discharge lasers," *Appl. Phys. Lett.*, vol. 33, pp. 171–173, 1978.
[9] R. T. Hawkins, H. Egger, J. Bokor, and C. K. Rhodes, "A tunable ultrahigh spectral brightness KrF excimer laser source," *Appl. Phys. Lett.*, vol. 36, pp. 391–392, 1980; and J. C. White, J. Bokor, R. R. Freeman, and D. Henderson, "Tunable ArF excimer laser source," *Opt. Lett.*, vol. 6, pp. 293–294, 1981.
[10] W. E. Ernst and F. K. Tittel, "A new electron-beam pumped XeF laser at 486 nm," *Appl. Phys. Lett.*, vol. 35, pp. 36–37, 1979.
[11] F. K. Tittel, W. L. Wilson, R. E. Stickel, G. Marowsky, and W. E. Ernst, "A triatomic Xe_2Cl excimer laser in the visible," *Appl. Phys. Lett.*, vol. 36, pp. 405–407, 1980.
[12] F. K. Tittel, G. Marowsky, M. C. Smayling, and W. L. Wilson, "Blue laser action by the rare gas halide trimer Kr_2F," *Appl. Phys. Lett.*, vol. 37, pp. 862–864, 1980.
[13] D. C. Lorents, D. L. Huestis, M. V. McCusker, H. H. Nakano, and R. M. Hill, "Optical emissions of triatomic rare gas halides," *J. Chem. Phys.*, vol. 68, pp. 4657–4661, 1978.
[14] G. Marowsky, R. Cordray, F. K. Tittel, and W. L. Wilson, "Versatile high-temperature high-pressure vapor cell design for electron beam excited laser studies," *Appl. Opt.*, vol. 17, pp. 3491–3495, 1978.
[15] W. K. Bischel, H. H. Nakano, D. J. Eckstrom, R. M. Hill, D. L. Huestis, and D. C. Lorents, "A new blue-green excimer laser in XeF," *Appl. Phys. Lett.*, vol. 34, pp. 565–567, 1979.
[16] N. G. Basov, V. S. Zuev, A. V. Kanaev, L. D. Mikkeev, and D. B. Stavrovskii, "Laser action due to the bound-free C(3/2)–A(3/2) transition in the XeF molecule formed by photodissociation," *Sov. J. Quantum Electron.*, vol. 9, p. 629, 1979.
[17] J. D. Campbell, C. H. Fischer, and R. E. Center, "Observation of gain and laser oscillations in the blue-green during direct pumping of XeF by microsecond electron beam pulses," *Appl. Phys. Lett.*, vol. 37, pp. 348–350, 1980.
[18] R. Burnham, "A discharge pumped laser on the *C->A* transition of XeF," *Appl. Phys. Lett.*, vol. 35, pp. 48–49, 1979.
[19] C. H. Fisher, R. E. Center, G. J. Mullaney, and J. P. McDaniel, "A 490-nm XeF discharge laser," *Appl. Phys. Lett.*, vol. 35, pp. 26–28, 1979.
[20] D. L. Huestis, "Tunable visible rare gas halide lasers," presented at the 1980 Lasers Conf., New Orleans, LA, Dec. 15–19, 1980.
[21] C. H. Fisher, R. E. Center, G. J. Mullaney, and J. P. McDaniel, "Multipass amplification and tuning of the blue-green XeF $C \rightarrow A$ laser," *Appl. Phys. Lett.*, vol. 35, pp. 901–903, 1979.
[22] W. E. Ernst and F. K. Tittel, "Gain studies of electron beam excited XeF laser mixtures," *IEEE J. Quantum Electron.*, vol. QE-16, pp. 945–948, Sept. 1980.
[23] R. M. Hill, P. L. Trevor, D. L. Huestis, and D. C. Lorents, "Measurement of gain on the XeF (C-A) blue-green band," *Appl. Phys. Lett.*, vol. 34, pp. 137–139, 1979.
[24] G. Marowsky, F. K. Tittel, W. L. Wilson, and E. Frenkel, "Laser gain measurements by means of amplified stimulated spontaneous emission," *Appl. Opt.*, vol. 19, pp. 138–143, 1980.
[25] D. Kligler, H. H. Nakano, D. L. Huestis, W. K. Bischel, R. M. Hill, and C. K. Rhodes, "Energy ordering of the excited states of XeF," *Appl. Phys. Lett.*, vol. 33, pp. 39–41, 1978.
[26] T. G. Finn, L. J. Palumbo, and L. F. Champagne, "The role of the C state in the XeF laser," *Appl. Phys. Lett.*, vol. 34, pp. 52–55, 1979.
[27] M. Rokni, J. H. Jacob, J. C. Hsia, and D. W. Trainor, "The origin of the broadband emission of XeF," *Appl. Phys. Lett.*, vol. 35, pp. 729–731, 1979.
[28] W. K. Bischel, D. J. Eckstrom, D. L. Huestis, and D. C. Lorents, "Photolytically pumped XeF (*C->A*) blue-green laser," presented at the 1979 Lasers Conf., Orlando, FL, Dec. 17–21, 1979; also in *J. Appl. Phys.*, vol. 52, pp. 4429–4434, 1981.
[29] W. E. Ernst and F. K. Tittel, "XeF laser characteristics studied at elevated temperatures," *J. Appl. Phys.* vol. 51, pp. 2432–2435, 1980.
[30] J. Leigel, F. K. Tittel, W. L. Wilson, and G. Marowsky, "Broad spectral tuning of an e-beam pumped XeF (*C->A*) laser," *Appl. Phys. Lett.*, vol. 39, pp. 369–371, 1981.
[31] G. Marowsky, M. Munz, and F. K. Tittel, "Excimer laser gain by pulse-shape analysis," *IEEE J. Quantum Electron.*, vol. QE-17, pp. 1281–1285, July 1981.
[32] G. Haag and G. Marowsky, "Transmission of organic laser dyes under inclusion of stimulated emission," *IEEE J. Quantum Electron.*, vol. QE-16, pp. 890–897, Aug. 1980.
[33] J. A. Mangano, J. H. Jacob, M. Rokni, and A. Hawryluk, "Three-body quenching of KrF* by Ar and broad-band emission at 415 nm," *Appl. Phys. Lett.*, vol. 31, pp. 26–28, 1977.
[34] N. G. Basov, V. A. Danilychev, V. A. Dolgikh, O. M. Kerimov, V. S. Lebedev, and A. G. Molchanov, "New excimer emission bands of noble-gas halides," *JETP Lett.*, vol. 26, pp. 16–19, 1977.
[35] V. S. Zuev, A. V. Kanaev, L. D. Mikheev, and D. B. Stavrov, "Blue luminescence mechanism of ArKrF* and KrN_2F excimers," *Sov. J. Quantum Electron.*, vol. 7, pp. 1562–1563, 1980.
[36] W. R. Wadt and P. J. Hay, "Electronic states of Ar_2F and Kr_2F," *J. Chem. Phys.*, vol. 68, pp. 3850–3863, 1978.
[37] C. F. Bender and H. F. Schaefer, III, "Ionic excited states of Ne_2F," *Chem. Phys. Lett.*, vol. 53, pp. 27–30, 1978.
[38] H. H. Michels, R. H. Hobbs, and L. A. Wright, "The electronic structure of ArF and Ar_2F," *Chem. Phys. Lett.*, vol. 48, pp. 158–161, 1977.
[39] W. R. Wadt and P. J. Hay, "The low-lying electronic states of Ar_2F," *Appl. Phys. Lett.*, vol. 30, pp. 573–575, 1977.
[40] D. L. Huestis and N. E. Schlotter, "Diatomics-in-molecules potential surfaces for the triatomic rare gas halides: Rg_2X," *J. Chem. Phys.*, vol. 69, pp. 3100–3107, 1978.
[41] N. G. Basov, V. S. Zuev, A. V. Kanaev, L. D. Mikheev, and D. B. Stavrovskii, "Laser action in an optically pumped Kr_2F triatomic excimer," *Sov. J. Quantum Electron.*, vol. 7, pp. 2660–2661, 1980.
[42] E. Zamir, D. L. Huestis, H. H. Nakano, R. M. Hill, and D. C. Lorents, "Visible absorption by electron-beam pumped rare gases," *IEEE J. Quantum Electron.*, vol. QE-15, pp. 281–288, 1979.
[43] G. Marowsky, G. P. Glass, M. C. Smayling, F. K. Tittel, and W. L. Wilson, "Dominant formation and quenching kinetics of electron beam pumped Xe_2Cl," *J. Chem. Phys.*, vol. 75, pp. 1153–1158, 1981.
[44] D. L. Huestis, "Studies of the triatomic rare gas halides," presented at the 1979 Top. Meeting Excimer Lasers, Charleston, SC, Sept. 11–13, 1979.
[45] K. Y. Tang and D. C. Lorents, "Studies of excimer laser excited kinetics using synchrotron radiation," presented at the 1980 Lasers Conf., Orleans, LA, Dec. 15–17, 1980.
[46] V. H. Shui and C. Duzy, "Theoretical study of the formation rates of rare-gas halide trimers," *Appl. Phys. Lett.*, vol. 36, pp. 135–136, 1980.
[47] D. L. Huestis, R. M. Hill, D. J. Eckstrom, M. V. McCusker, D. C. Lorents, H. H. Nakano, B. E. Perry, J. A. Margevicius, and N. E. Schlotter, "New electronic transition laser systems," SRI Int., Menlo Park, CA, SRI Project PYU-6158, Tech. Rep. 1, 1978.
[48] G. P. Quigley and W. M. Hughes, "Lifetime and quenching rate constants for KR_2F* and KR_2*," *Appl. Phys. Lett.*, vol. 32, pp. 649–651, 1978.
[49] C. H. Chen and M. G. Payne, "Ar_2F radiative lifetime measurement," *Appl. Phys. Lett.*, vol. 32, pp. 358–360, 1978; and C. H. Chen, M. C. Payne, and J. P. Judish, "Kinetic studies of ArF* and Ar_2F* in proton excited Ar-F_2 mixtures," *J. Chem. Phys.*, vol. 69, pp. 1626–1635, 1978.
[50] K. L. Hohla, T. R. Loree, C. A. Brau, and W. E. Stein, "A linac pumped excimer laser: Fluorescence and scaling studies," *Appl. Phys.*, vol. 25, pp. 329–336, 1981.
[51] G. P. Glass, F. K. Tittel, W. L. Wilson, M. C. Smaying, and G. Marowsky, "Quenching kinetics of electron beam pumped XeCl," *Chem. Phys. Lett.*, to be published.
[52] H. C. Brashears, Jr., D. W. Setser, and Y. C. Yu, "Emission spectra of KrXeCl*, KrXeBr*, KrXeI*, ArKrF*, and ArKrCl*," *J. Chem. Phys.*, vol. 74, pp. 10–17, 1981.
[53] R. O. Hunter, J. Oldenettel, C. Howton, and M. V. McCusker, "Gain measurements at 4416 A on ArXeF* and Kr_2F*," *J. Appl. Phys.*, vol. 49, pp. 549–552, 1978.
[54] J. G. Eden, R.S.F. Chang, and L. J. Palumbo, "Absorption in the near ultraviolet wing of the Kr_2F* (410 nm) band," *IEEE J. Quantum Electron.*, vol. QE-15, pp. 1146–1156, 1979.
[55] K. Y. Tang, D. C. Lorents, and D. L. Huestis, "Gain measurements on the triatomic excimer Xe_2Cl," *Appl. Phys. Lett.*, vol. 36, pp. 347–349, 1980.
[56] J. K. Rice, G. C. Tisone, and E. L. Patterson, "Oscillator performance and energy extraction from a KrF laser pumped by a high intensity relativistic electron beam," *IEEE J. Quantum Electron.*, vol. QE-16, pp. 1315–1326, Dec. 1980.
[57] L. F. Champagne and R.S.F. Chang, "Transient absorption studies in pure rare gases from 2500 A to 4000 A," *J. Phys.*, vol. 41, C9, pp. 445–447, 1980.

[58] R. F. Stebbings, C. J. Latimer, W. P. West, F. B. Dunning, and T. B. Cook, "Studies of xenon atoms in high Rydberg states," *Phys. Rev. A*, vol. 12, pp. 1453–1458, 1975.
[59] R. D. Rundel, F. B. Dunning, H. C. Goldwire, Jr., and R. F. Stebbings, "Near-threshold photoionization of xenon metastable atoms," *J. Opt. Soc. Amer.*, vol. 65, pp. 628–633, 1975.
[60] R. F. Stebbings and F. B. Dunning, "Autoionization from high-lying $3p^5$ $(^2P_{1/2})$ np' levels in argon*," *Phys. Rev. A*, vol. 8, p. 665, 1973.
[61] M. Bourene, and J. LeCalve, "De-excitation cross-sections of metastable argon by various atoms and molecules," *J. Chem. Phys.*, vol. 58, p. 1452, 1973.
[62] R. E. Gleason, T. D. Bonifield, J. W. Keto, and G. K. Walters, "Electronic energy transfer in argon-xenon mixtures excited by electron bombardment," *J. Chem. Phys.*, vol. 66, pp. 1589–1593, 1977; and C. A. Brau, *Excimer Lasers*, C. K. Rhodes, Ed. Berlin: Springer, 1979, ch. 4.
[63] C. E. Moore, *Atomic Energy Levels*, vol. III, Nat. Bur. Standards, Circ. 467, U.S. Gov. Printing Office, Washington, DC, 1958.
[64] M. Rokni, J. H. Jacob, and J. A. Mangano, "Dominant formation and quenching processes in e-beam pumped ArF* and KrF* lasers," *Phys. Rev. A*, vol. 16, pp. 2216–2224, 1977.
[65] S. C. Lin and J. I. Levatter, "X-ray preionization for electric discharge lasers," *Appl. Phys. Lett.*, vol. 34, pp. 505–508, 1979.
[66] B. Forestier, B. Fontaine, and P. Gross, "Supersonic flow low temperature electronic transition excimer laser," *J. Phys.*, vol. 41, C9, pp. 455–462, 1980.
[67] R. A. Klein, "λ-3, Sandia's 100J HF laser system," Sandia Nat. Lab., Alberquerque, NM, Rep. SAND 79-1659, Sept. 1979.
[68] R. Sauerbrey and H. Langhoff, "Lasing in an *e*-beam pumped Ar-N_2-mixture at 406 nm," *Appl. Phys.*, vol. 22, pp. 399–402, 1980.
[69] R. W. Dreyfus and R. T. Hodgson, "Molecular-hydrogen laser; 1098–1613 A," *Phys. Rev. A*, vol. 9, pp. 2535–2648, 1974.
[70] H. P. Grieneisen, H. Xue-Ting, and K. L. Kompa *Chem. Phys. Lett.*, to be published.

Frank K. Tittel (SM'72), for a photograph and biography, see p. 1285 of the July 1981 issue of this JOURNAL.

Gerd Marowsky, for a photograph and biography, see p. 356 of the March 1981 issue of this JOURNAL.

William L. Wilson, Jr. (S'68–M'71) was born in Bay Shore, NY, on February 6, 1943. He received the B.S. degree in 1965, the M.E.E. degree in 1966, and the Ph.D. degree in 1972, all in electrical engineering, from Cornell University, Ithaca, NY.

From 1971 to 1972 he was an Instructor-Research Associate with the Department of Electrical Engineering at Cornell. In 1972 he became an Assistant Professor of Electrical Engineering at Rice University, Houston, TX, where he is currently an Associate Professor. His research interests include far-infrared devices and thin-film magnetic materials.

Dr. Wilson is a member of Tau Beta Pi, Eta Kappa Nu, Sigma Xi, the IEEE Magnetics Society, the IEEE Microwave Theory and Techniques Society, and the IEEE Electron Devices Society.

Michael C. Smayling was born on August 31, 1952, in Kansas City, KS. He received the B.E.E. degree from the University of Minnesota, Minneapolis, and the M.S. and Ph.D. degrees in electrical engineering from Rice University, Houston, TX, in 1972, 1976, and 1981, respectively.

He was with the du Pont Company, Victoria, TX, in 1973, transferring to the du Pont Experimental Station in 1976. His work included electrooptical instrument design and design of a clinical patient identification system to be used with the du Pont "aca" (patent pending). He is currently a Staff Member of Texas Instruments, Houston, TX. His present interests include VLSI process development, submicron transistor characterization, plasma kinetics, and laser chemistry. He is a Licensed Professional Engineer.